AJNR

# Diffusion-Weighted MR Imaging of the Spinal Cord

Roland Bammer, Franz Fazekas, Michael Augustin, Josef Simbrunner, Siegrid Strasser-Fuchs, Thomas Seifert, Rudolf Stollberger and Hans-Peter Hartung

*AJNR Am J Neuroradiol* 2000, 21 (3) 587-591
http://www.ajnr.org/content/21/3/587

*AJNR Am J Neuroradiol* 21:587–591, March 2000

**Technical Note**

# Diffusion-Weighted MR Imaging of the Spinal Cord

Roland Bammer, Franz Fazekas, Michael Augustin, Josef Simbrunner, Siegrid Strasser-Fuchs, Thomas Seifert, Rudolf Stollberger, and Hans-Peter Hartung

**Summary: Diffusion-weighted MR imaging may increase the sensitivity and specificity of MR imaging for certain pathologic conditions of the spinal cord but is rarely performed because of several technical issues. We therefore tested a novel phase-navigated spin-echo diffusion-weighted interleaved echo-planar imaging sequence in seven healthy volunteers and six patients with intramedullary lesions. We performed diffusion-weighted MR imaging of the spinal cord with high spatial resolution. Different patterns of diffusion abnormalities observed in patient studies support the possible diagnostic impact of diffusion-weighted MR imaging for diseases of the spinal cord.**

MR imaging has become the technique of choice for imaging the spinal cord because of a high sensitivity for pathologic intramedullary changes (1). Nonetheless, the specificity of abnormalities frequently lags behind when using only conventional MR sequences. Diffusion-weighted MR imaging (2) promises to supply further information because of characteristic changes of the apparent diffusion coefficient, such as those manifested in acute ischemia, tumors, or lesions associated with multiple sclerosis (3). To date, the diagnostic contribution of diffusion-weighted MR imaging has been studied primarily in the brain because diffusion-weighted MR imaging of the spine is technically more demanding. Both the small size of the spinal cord and motion-induced artifacts must be considered. We therefore developed a new examination technique and tested its reliability and potential for contributing to the diagnostic workup of patients with spinal cord symptoms.

## Description of the Technique

All studies were performed on a 1.5-T Philips Gyroscan ACS-NT (Philips Medical Systems; Best, Netherlands) with self-shielded gradients ($G_{max} = 23 - mTm^{-1}$, slew rate = $105 - Tm^{-1}s^{-1}$). RF excitation was achieved by using the circularly polarized whole-body resonator, while either a circularly polarized neck coil or a circularly polarized phased-array coil, depending on the region to be imaged, was used for signal reception.

For diffusion imaging, we used a phase-navigated interleaved echo-planar imaging method (4). The diffusion-weighted sequences were RR-gated by using the plethysmographic signal from a finger-pulse oximeter triggered from every second R-peak to avoid artifacts from the movement of the spinal cord and the pulsation of CSF. Moreover, to prevent influences of moving structures, oblique saturation slabs were placed in the pharynx and thoracic cave region. Additionally, a spectral fat-saturation pulse was used to suppress the artifacts arising from lipid tissue (ie, chemical shift). Because of segmented k-space acquisition, the echo time–shift technique was applied (5) to reduce modulations of the phase error function in k-space that otherwise lead to ghosting artifacts. The sequence parameters for diffusion-weighted MR imaging were as follows: ~1500/87/4 (TR/TE/excitations); imaging matrix, 192 × 256; field of view, 161 × 230 mm; partial Fourier imaging; number of gradient echoes per echo-planar imaging interleaf factor, 11; section thickness/gap, 3.5/0.35 mm; and number of sections, 7. The duration, $\delta$, of one diffusion gradient pulse was 28 ms. The time between the leading edges of both diffusion gradient pulses, $\Delta$, was 37 ms. $B_0$-inhomogeneities were corrected by means of a vendor-specific automatic shimming procedure. For phase navigation, the nonlinear method presented by de Crespigny et al (6) was used, which provides phase correction for both translational and rotational movement. The correction was performed immediately after data acquisition during image reconstruction. The method that was used performs phase correction in hybrid space after 1D-Fourier transformation of the acquired data in readout direction. One navigator projection in hybrid space was chosen as a reference view for calculating the relative phase perturbations of the remaining views, reflecting the random motions of the participant.

The diffusion attenuation (b-values) values used were approximately 0 and 709 s/mm. Diffusion-weighted MR imaging measurements were obtained with diffusion weighting along each principal axis (anteroposterior, left-right, and cephalocaudal) and with sagittal section order. Further postprocessing was performed off-line using an in-house dedicated MR image-processing software. The apparent diffusion coefficient, ADC, was calculated on a per-pixel basis according to the following characteristic equation:

$$ADC = \frac{1}{b}(\ln S_0 - \ln S_b), \quad (1)$$

where b is the diffusion-weighting factor, $S_b$ is the diffusion-weighted signal, and $S_0$ is the signal intensity when the diffusion gradients were turned off. Moreover, in our volunteer study, the trace of the diffusion tensor was used, which evaluates the following:

$$Tr(\mathbf{D}) = \sum_{i=AP,LR,CC} ADC_i, \quad (2)$$

where AP, LR, and CC, indicate diffusion weighting along the

Received July 8, 1999; accepted after revision October 11.

From the Department of Neurology (R.B., F.F., M.A., S.S.-F., T.S., H.-P.H.) and the Magnetic Resonance Institute (R.B., F.F., M.A., J.S., R.S.), Karl-Franzens University, Graz, Austria.

Address reprint requests to Franz Fazekas, MD, Department of Neurology, Karl-Franzens University, Graz, Auenbruggerplatz 18, A-8036 Graz/Europe.

This work was supported in part by grant GHS-319/94 from the Gemeinnützige Hertie Stiftung (Frankfurt, Germany).

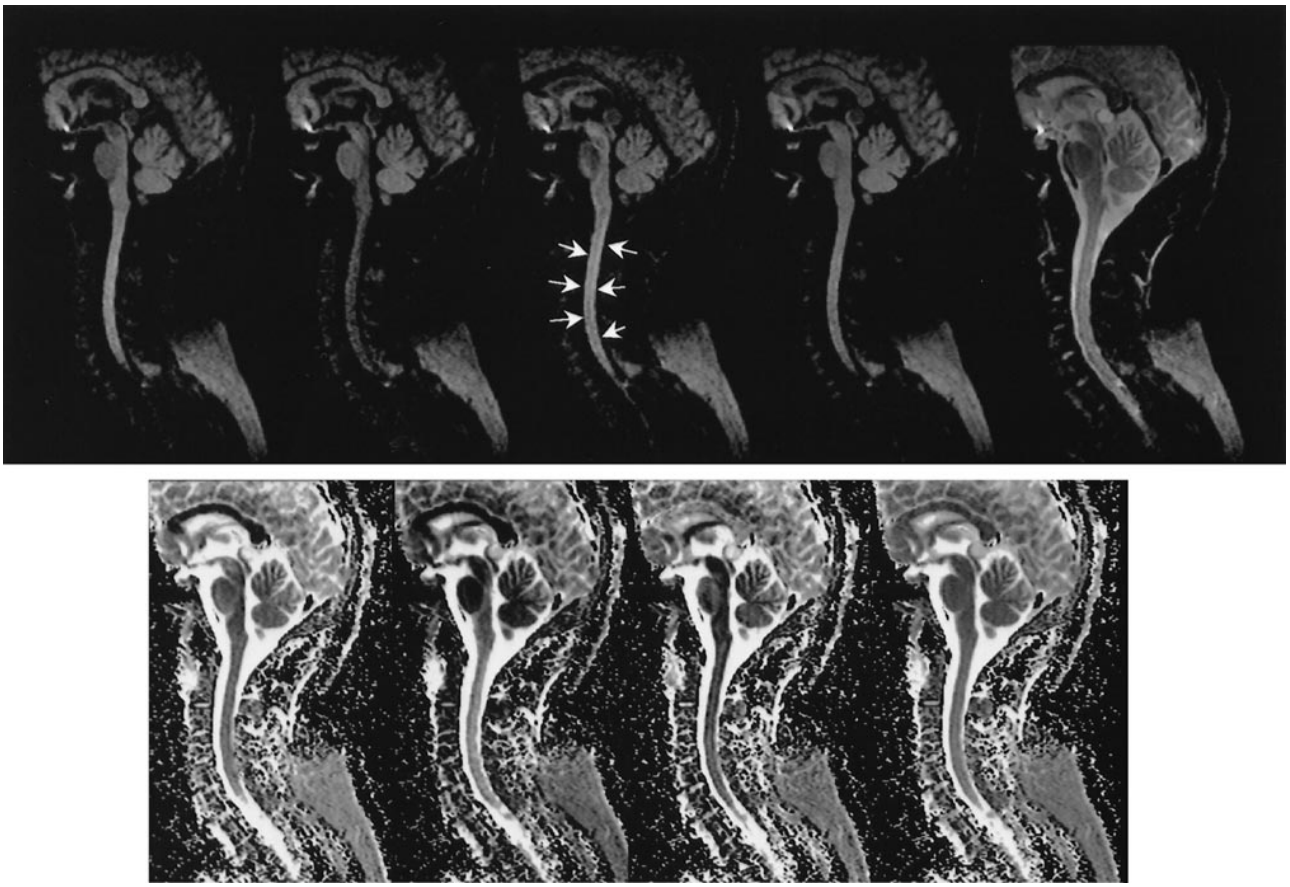

FIG 1. Diffusion-weighted images obtained from volunteers in three mutually orthogonal directions.

*Top row,* Direction-dependent diffusion-weighted interleaved echo-planar images of the cervical spine in a healthy male volunteer (images 1 to 3) with corresponding calculated trace-weighted diffusion and T2-weighted interleaved echo-planar images (images 4 and 5, from *left* to *right*). Diffusion gradients were applied in anteroposterior, cephalocaudal, and left-right directions (from *left* to *right*) at a b-value of 709 s/mm.

*Bottom row,* Calculated maps of apparent diffusion coefficient for diffusion weighting along anteroposterior, cephalocaudal, and left-right directions and trace of the diffusion tensor (from *left* to *right*).

Diffusion anisotropy can be clearly appreciated in the corpus callosum, the pontine region, and the spinal cord itself. Contrast between gray and white matter is most apparent with diffusion weighting in the left-right direction (*arrows*).

anteroposterior, left-right, and cephalocaudal directions. Ultimately, trace-weighted diffusion images, $S_{Trace}$, were calculated according to the following equation:

$$S_{Trace} = \sqrt[3]{S_{AP}S_{LR}S_{CC}}, \quad (3)$$

where $S_{AP}$, $S_{LR}$, and $S_{CC}$ are the diffusion-weighted signal intensities with weighting along the anteroposterior, left-right, and cephalocaudal axes. Image analysis was performed independently by skilled operators (M.A., R.B.) on a region-of-interest basis.

Conventional imaging comprised T2-weighted fast spin-echo (2700/110/3; number of echoes per interleaf, 17) and unenhanced and contrast-enhanced T1-weighted fast spin-echo sequences (525/13.8/3; number of echoes per interleaf, 4) with geometric parameters identical to those of the diffusion imaging.

We examined seven volunteers who were free of neurologic disease and whose ages ranged from 24 to 35 years (28.6 ± 3.65 years). These examinations served to test the reliability of our technique and to obtain diffusion measurements. For clinical studies, we selected six patients (five female patients and one male patient) with known spinal cord pathologic abnormalities whose ages ranged from 35 to 65 years. Because of time constraints in the patient studies, diffusion encoding was performed in one direction only. Informed consent was obtained after the nature of the procedures had been fully explained, before the MR imaging procedure was performed. The imaging protocols were approved by our institution's committee on human studies.

## Discussion

To date, diffusion characteristics of the spinal cord have been studied primarily in animals, either in vivo (7) or in vitro on excised specimens (8), and most of these studies were conducted on small-bore systems in conjunction with MR microscopy equipment. Studies of humans have suffered from technical problems, such as the high susceptibility to resonance offsets (eg, $B_0$-inhomogeneities, susceptibility gradients, chemical shift) and inherently low spatial resolution of single-shot echo-planar imaging or limited spatial resolution, long acquisition time, and low signal-to-noise ratios in the case of fast spin-echo-based techniques (9) or line scan diffusion imaging (10). Furthermore, artifacts arising from CSF pulsatile flow, swallowing as well

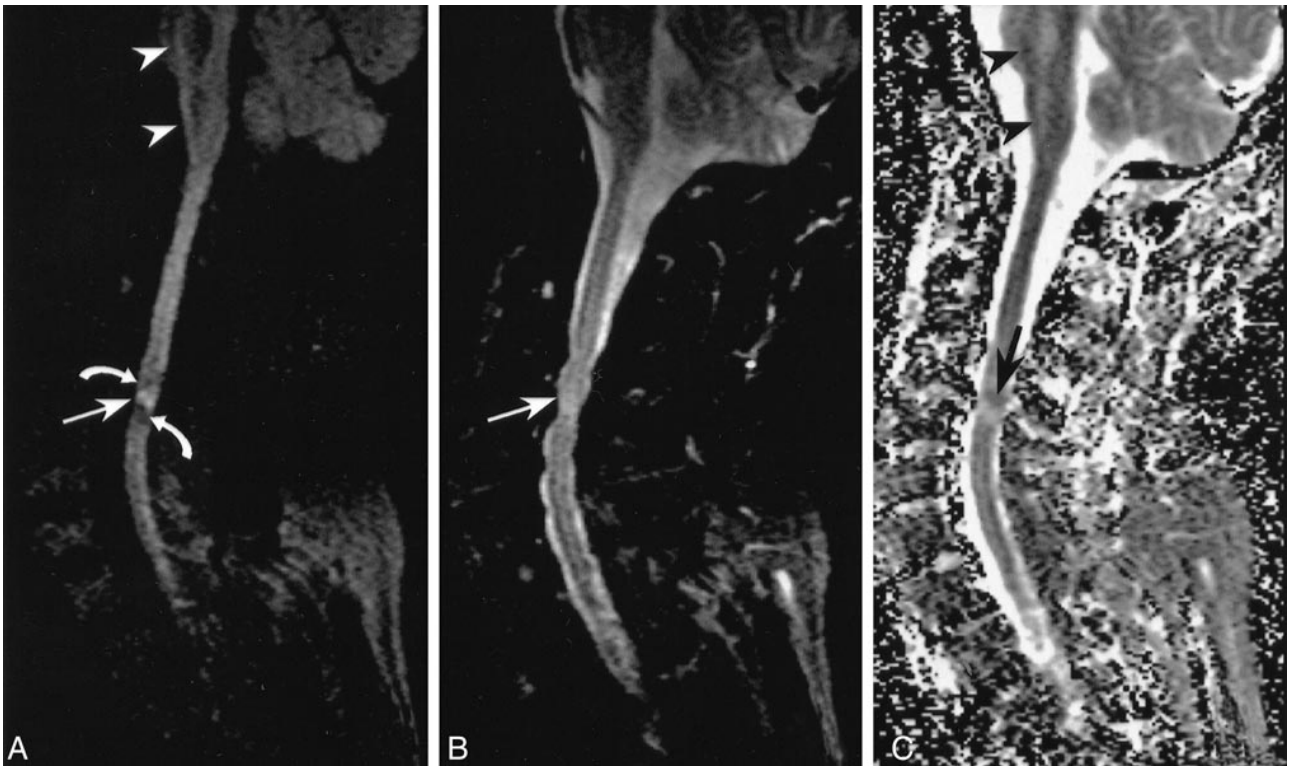


FIG 2. Images of a 41-year-old male patient who was suffering from spondylotic myelopathy with evolution of spastic tetraparesis over the course of 3 to 4 weeks.

*A,* Diffusion-weighted interleaved echo-planar image clearly shows a hyperintense lesion (*straight arrow*) surrounded by a hypointense, presumably edematous, area (*curved arrows*).

*B,* T2-weighted interleaved echo-planar image shows corresponding hyperintensity (*straight arrow*).

*C,* Reduced diffusion, confirmed by a region of interest–based analysis of apparent diffusion coefficient maps, is likely caused by vascular compromise with cell swelling (*black arrow*). Note that fiber structures of the pyramidal tract running in a cephalocaudal direction are clearly apparent in the pontine region and medulla oblongata (*arrowheads*) because of left-right diffusion gradient application. Cord hyperintensity from C1 to the proximity of the lesion in *A* is from white matter anisotropy, similar to that observed in volunteers.

as breathing, may constitute serious problems for diffusion-weighted MR imaging of the spinal cord.

Considering all of these aspects, we used a novel phase-navigated high-resolution diffusion-weighted MR imaging method, which relies on an interleaved echo-planar imaging technique. The inherently increased k-space velocity of interleaved echo-planar imaging leads to a marked reduction of echo-planar imaging-specific artifacts in contrast to single-shot echo-planar imaging. This allowed for a good trade-off between echo-planar imaging–induced artifacts and acquisition time in our study. Measurements for two b-levels took approximately 4 to 5 minutes, depending on the patients' heart rates. The markedly lower acquisition time compared with standard navigated spin-echo diffusion-weighted imaging seems to be an important advantage regarding tolerance of the examination and a lower probability of motion artifacts. Using this technique, we obtained high-quality diffusion-weighted MR imaging of the spinal cord in volunteers and in patients.

Volunteer examinations, performed in three mutually orthogonal directions, yielded diffusion-weighted images of excellent quality (Fig 1). Region of interest–based measurement of the apparent diffusion coefficient in the cervical cord of volunteers yielded values similar to those reported in a previous study (9). The apparent diffusion coefficient perpendicular to the cord fibers was $(545 \pm 76) \times 10^{-6}$ mm/s (mean ± SD), whereas measurements parallel to the fiber tracts showed values of $(1603 \pm 82) \times 10^{-6}$ mm/s. This is consistent with the anisotropic diffusion characteristic of the human spinal cord. Despite high-resolution imaging, which allows separation between gray and white matter, a quantitative assessment of both compartments could not be achieved.

The clinical conditions examined were spinal cord tumor (n = 2), cervical spondylotic myelopathy (n = 2), anterior spinal artery infarction (n = 1), and myelitis (n = 1), with follow-up of the latter. Our first clinical results show the potential diagnostic usefulness of spinal cord diffusion-weighted MR imaging. Despite ghosting artifacts, subacute anterior spinal artery infarction was characterized by a bright lesion involving the anterior portion of the spinal cord. From experience in the brain, it can be speculated that diffusion-weighted MR imaging should allow detection of such lesions also in the very early phase of spinal cord ischemia, which currently is not possible with conventional

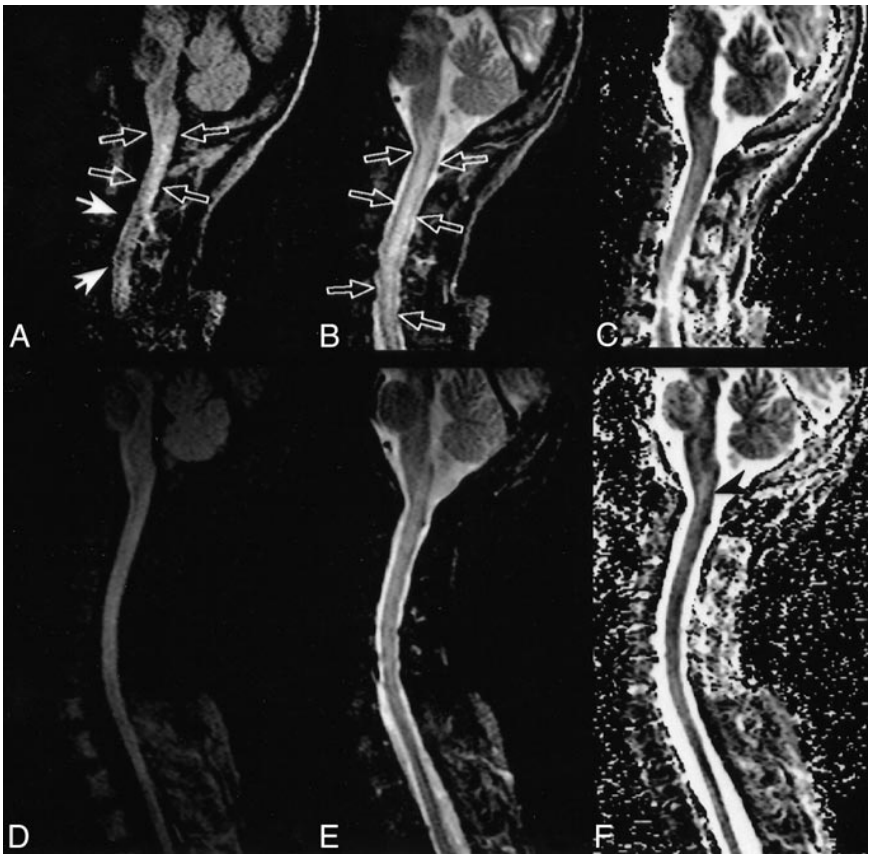


FIG 3. Only mild hyperintensity was seen on diffusion-weighted MR images of a patient with myelitis.

*A,* Diffusion-weighted interleaved echo-planar image shows diffuse signal hyperintensity and swelling of the cervical spinal cord (*open arrows*). Note the signal cancellation due to ghosting artifacts (*closed arrows*) caused by bulk motion.

*B,* T2-weighted interleaved echo-planar image shows diffuse signal hyperintensity and swelling of the cervical spinal cord (*open arrows*), consistent with myelitis.

*C,* Region-of-interest measurements on corresponding apparent diffusion coefficient maps reveal moderately increased apparent diffusion coefficient values. Therefore, hyperintensity in diffusion-weighted MR imaging seems to be related to the so-called ''T2-shine-through'' effect that compensates for increased apparent diffusion coefficient.

*D,* Diffusion-weighted interleaved echo-planar image obtained at follow-up 7 months later. No pathologic signal alteration is seen.

*E,* T2-weighted interleaved echo-planar image obtained at follow-up 7 months later. The cord volume appears normal, and only faint intramedullary hyperintensities have remained.

*F,* Apparent diffusion coefficient map shows a small area with elevated apparent diffusion coefficient at the level between the medulla oblongata and C1 (*arrowhead*), which may represent residual damage.

MR sequences (11). Less expectedly, bright intramedullary hyperintensities owing to apparent diffusion coefficient reduction were also seen in both patients with cervical spondylotic myelopathy (Fig 2). This finding seems to support vascular compromise with cell swelling as an important element in the evolution of clinical symptoms from degenerative spine disease with only mild cord compression (12). Because of markedly elevated apparent diffusion coefficient (Fig 2), the observed rim of hypointensity at the periphery on diffusion-weighted MR images most likely indicates edema. Only mild hyperintensity was seen on diffusion-weighted MR images of myelitis (Fig 3). In this context, the increase in signal was related to T2 hyperintensity, whereas the apparent diffusion coefficient was actually moderately increased in that particular region. This may suggest the possibility of separating ischemic from inflammatory cord lesions by means of diffusion-weighted MR imaging. Nonspecific patterns of signal change were seen on diffusion-weighted MR images of both patients with intramedullary tumors.

Despite all efforts, shimming and subsequent fat suppression were partly imperfect in some of our measurements, so that the fat-saturation pulse gradually tended to saturate water and leave fat-bound protons intact (Fig 1). Attempts to improve $B_0$-field homogeneity by using wrap-around pads, which were attached around the cervical region and contained an MR imaging-invisible gel with magnetic susceptibility identical to that of the human body, were of limited success. Implementation of simultaneous spatial and spectral excitation by means of water-only pulses might potentially help to circumvent this problem but was not available on our system. On several occasions, when image quality was insufficient, we turned off the fat saturation and reduced the number of gradient echoes per echo-planar imaging shot at the cost of moderately in-

creased acquisition time (an approximate increase of 1 min). Influences from partial volume effects emerging from CSF were minimized by using thin sections. In this context, CSF suppression techniques might be another option and proximal saturation slabs could help to reduce CSF pulsation artifacts.

Diffusion anisotropy is another issue that deserves consideration (Fig 1). Because of time constraints, we were unable to measure the complete trace of the diffusion tensor in our patients, but we used comparative regional apparent diffusion coefficient measurements from volunteers to overcome this deficit partially. Deviations from the symmetrical organization of the spinal cord and diffusion values in the vicinity of a lesion can also help to confirm abnormal findings. Certainly, measurements of the trace of the diffusion tensor would seem necessary to detect subtle changes. Accordingly, determination of the full diffusion tensor would be desirable for a more reliable characterization of diffusion anisotropy (10). Nonetheless, regarding the maximum of achievable signal-to-noise ratio, the implementation of such a technique seems difficult at present.

## References


1. Fazekas F, Kapeller P. **Diseases of the spinal cord.** In: Greenberg JO, ed. *Neuroimaging: A Companion to Adams and Victors Principles of Neurology.* 2nd ed. New York: McGraw-Hill; 1999:521–542
2. LeBihan D. **Molecular diffusion nuclear magnetic resonance imaging.** *Magn Reson Q* 1991;7:1–30
3. Moseley ME, Cohen Y, Mintorovich J, et al. **Early detection of regional cerebral ischemia in cats: comparison of diffusion- and T2-weighted MRI and spectroscopy.** *Magn Reson Med* 1990;14:330–346
4. Bammer R, Stollberger R, Augustin M, et al. **Diffusion-weighted imaging with navigated interleaved echo-planar imaging and a conventional gradient system.** *Radiology* 1999;211:799–806
5. Feinberg DA, Oshio K. **Phase errors in multi-shot echo planar imaging.** *Magn Reson Med* 1994;32:535–539
6. de Crespigny AJ, Marks MP, Enzmann DR, Moseley ME. **Navigated diffusion imaging of normal and ischemic human brain.** *Magn Reson Med* 1995;33:720–728
7. Moseley ME, Cohen Y, Kucharczyk J, et al. **Diffusion-weighted MR imaging of anisotropic water diffusion in cat central nervous system.** *Radiology* 1990;176:439–445
8. Pattany PM, Puckett WR, Klose KJ, Quencer RM, Bung RP, Weaver RG. **High-resolution diffusion-weighted MR of fresh and fixed cat spinal cords: evaluation of diffusion coefficients and anisotropy.** *AJNR Am J Neuroradiol* 1997;18:1049–1056
9. Yamada H, Okubo T, Abe O, et al. **Diffusion-weighted imaging of the cervical spine with single shot fast spin echo (SSFSE) sequence.** In: *Book of Abstracts: International Society of Magnetic Resonance in Medicine 1999.* vol 3. Philadelphia: International Society of Magnetic Resonance in Medicine; 1999:1816
10. Zientara GP, Murphy BP, Maier SE, et al. **Diffusion tensor MRI of the human cervical spinal cord in vivo in preterm newborns.** In: *Book of Abstracts: International Society of Magnetic Resonance in Medicine 1999.* Vol 2. Philadelphia: International Society of Magnetic Resonance in Medicine; 1999:1099
11. Yuh WT, Marsh EE III, Wang AK, et al. **MR imaging of spinal cord and vertebral body infarction.** *AJNR Am J Neuroradiol* 1992;13:145–154
12. Fehlings MG, Skaf G. **A review of the pathophysiology of cervical spondylotic myelopathy with insights for potential novel mechanisms drawn from traumatic spinal cord injury.** *Spine* 1998;23:2730–2737